The Astrophysical Journal, 668:1001–1011, 2007 October 20
© 2007. The American Astronomical Society. All rights reserved. Printed in U.S.A.

LABORATORY SIMULATION OF COMPETITION BETWEEN HYDROGENATION AND PHOTOLYSIS IN THE CHEMICAL EVOLUTION OF H_2O-CO ICE MIXTURES

N. Watanabe, O. Mouri, A. Nagaoka, T. Chigai, and A. Kouchi
Institute of Low Temperature Science, Hokkaido University, Sapporo, Hokkaido 060-0819, Japan; watanabe@lowtem.hokudai.ac.jp

and

V. Pirronello
D.M.F.C.I., Università di Catania, Viale A. Doria 6, 95125 Catania, Sicily, Italy; pirronello@dmfci.unict.it
Received 2007 January 24; accepted 2007 July 5

ABSTRACT

Hydrogenation and photolysis of H_2O-CO binary ice mixtures at 10–50 K have been revisited in order to quantitatively evaluate their relative importance in the chemical evolution of interstellar dust icy mantles. The dominant product of photolysis was CO_2, with lower yields of formaldehyde, methanol, and formic acid, while only formaldehyde and methanol were obtained by hydrogenation reactions. Hydrogenation has higher formation efficiencies and yields of formaldehyde and methanol than photolysis. However, the contribution of photolysis should not be negligible for the formation of these molecules in molecular clouds. The simultaneous irradiation of binary ice mixtures with hydrogen atoms and UV photons resulted in relative abundances of CO_2, formaldehyde, methanol, and formic acid that are consistent with the observed abundances. Our results show that the composition and structure of ice are crucial in the chemical evolution of ice mantles, as much as the temperature and the type of irradiation.

Subject headings: astrochemistry — dust, extinction — ISM: molecules — molecular processes

1. INTRODUCTION

Chemical processes occurring on dust grains play a crucial role in the formation of important interstellar molecules such as molecular hydrogen (H_2), carbon dioxide (CO_2), and several organic species. In particular, surface processes on dust grains in dense clouds that show the presence of "dirty ice" mantles, predominantly formed by H_2O, have been of interest to astrochemists, since various other molecules have also been found in such mantles. Most of these molecules, except carbon monoxide (CO) and few others, must be produced mainly by reactions in ice rather than in gas phase. Since the early 1980s, many experiments have been performed to simulate the chemical processing of interstellar ices by energetic processes, namely photolysis and ion bombardment, (e.g., Pirronello et al. 1982; d'Hendecourt et al. 1986; Schutte 1996 and references therein). Such experiments were able to produce a great many of the various molecules observed in icy mantles. However, these experiments did not address the elementary processes and their cross sections in great quantitative detail, especially since they were performed on rather complex ice mixtures. It in any case became clear that these processes must be very effective under the strong radiation field conditions. However, in dense interstellar regions where the UV photon field is weak, nonenergetic surface reactions between molecules and atoms, such as H and O, become important. Experiments on surface reactions started in the 1990s (e.g., Pirronello et al. 1997b; Hiraoka et al. 1994). Because of the intrinsic difficulties in producing and handling radical atoms, some of the early experiments were substantially qualitative; thus, sticking coefficients, diffusion constants of atoms on the surface, and exact rate constants could not be obtained from these experiments. However, other experiments (e.g., Pirronello et al. 1997a, 1999; Vidali et al. 2004; Watanabe et al. 2006; Watanabe 2006) provided efficiencies and *effective* rate constants or energy barriers for the surface reactions, which enable us to verify the practical relevance of those reactions under the various conditions in molecular clouds. In interstellar environments, energetic processes and surface reactions compete with each other. Therefore, to gain a quantitative understanding of the chemical evolution, we first studied the single process and then the superposition of the two processes.

In the present paper, we focus our attention on the formation processes of CO_2 and the simplest organic molecules, formaldehyde (H_2CO) and methanol (CH_3OH). These molecules are found abundantly in ice mantles and are important precursors of more complex prebiotic species. It is well known that those molecules are produced in the photolysis (Allamandola et al. 1988; Schutte et al. 1999) of ice mixtures containing H_2O and CO. Schutte et al. (1996) reported that the photolysis of ice is insufficient to explain the observed abundances in interstellar ices. However, the experiments on which such an argument was based were not quantitative enough (Schutte 1988) or were performed using too complex multicomponent ice mixtures (d'Hendecourt et al. 1986). Although Watanabe & Kouchi (2002a) did not detect a significant presence of products other than CO_2 in their experiment on the photolysis of H_2O-CO binary ice, the signal-to-noise ratio obtainable with the apparatus used in that study was not high enough to observe minor products. Another energetic process, proton bombardment of H_2O-CO ice, was studied experimentally by Hudson & Moore (1999). They demonstrated that this process would be effective in producing CH_3OH in cometary nuclei only over a cosmic-ray irradiation of 4.6 billion years. Recently, it was revealed experimentally that H_2CO and CH_3OH can be produced efficiently by the successive hydrogenation of CO on surfaces at temperatures that are typical in molecular clouds (Watanabe & Kouchi 2002b; Watanabe et al. 2003, 2004). This process had already been proposed on theoretical grounds (e.g., Tielens & Whittet 1997; Charnley et al. 1997). As described above, and in spite of the several studies on the formation of H_2CO and CH_3OH in ice mantles, a quantitative comparison between the relative efficiency of energetic processes and surface reactions has not yet been made. Furthermore, the dependence of these processes on the composition and the structure of the ice have not been reported in detail. To quantitatively evaluate the competing processes on the various types of ice mantles in molecular clouds, experiments on those processes should be performed under controlled conditions, using

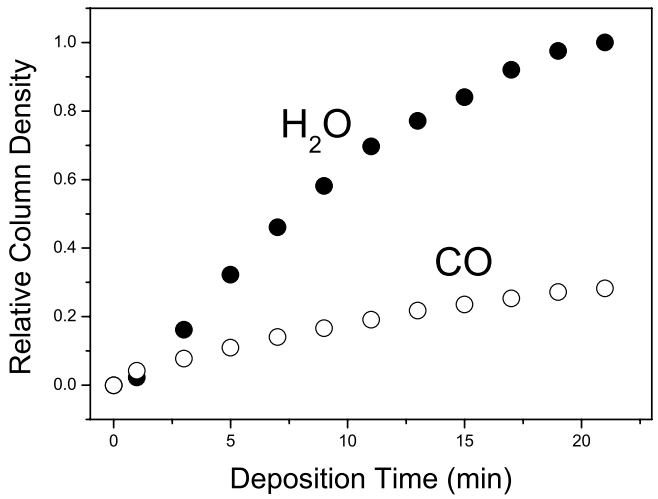


FIG. 1.—Growth of H_2O-CO mixed ice on the substrate during deposition at 15 K. The *y*-axis is a relative column density normalized to the final column density of H_2O.

the same and simple composition of samples, measuring the fluences of radiation and atoms, and changing the composition and structure of samples.

Here we report the results of three types of experiments: UV irradiation, thermal hydrogen atom exposure, and the superposition of the two processes (called co-irradiation) of ice mantle analogs H_2O-CO mixed ice and CO-capped ice.

2. EXPERIMENTAL

The apparatus used in the present experiments was newly constructed, with a design similar to ASURA (Nagaoka et al. 2005, 2007; Watanabe et al. 2006) and LASSIE (Watanabe et al. 2004). Briefly, the apparatus consists of an atomic source and a main chamber. The atomic chamber is evacuated by a turbomolecular pump (TG-900M, Osaka Vacuum; 900 liters s^{-1}), and the atomic source chamber is differentially pumped. The base pressure of the main chamber is approximately 3×10^{-10} torr, but it reaches a few $\times 10^{-7}$ torr during beam operation. A mirror-polished aluminum substrate connected to a cold head is positioned at the center of the main chamber. The sample area is surrounded by a copper shroud cooled by liquid nitrogen to obtain a high pumping speed for H_2O. Sample solids were created on the substrate by vapor deposition through a capillary plate forming an incident angle of 60° with the surface of the substrate. The composition of ice was measured by a Fourier-transform infrared (FTIR) spectrometer (PerkinElmer, Spectrum One) with a resolution of 4 cm^{-1}. Two types of samples were used in the present experiment: (1) a H_2O-CO intimate ice mixture prepared in the gas phase and then deposited on the cold substrate (hereafter referred to as "mixed ice") with the ratio of $H_2O/CO \sim 4$, and (2) a pure H_2O ice layer with 1 monolayer (ML) of CO on top (hereafter referred to as "CO-capped ice"). The thicknesses of the mixed ice and CO-capped ice were approximately 30 monolayer (ML). In the deposition conditions of the present experiment, the ice samples have amorphous structure. Since the surface of the amorphous ice is very rough, we use the expression "monolayer" to mean the amount of CO creating 10^{15} molecules cm^{-2}, rather than the usual idea of a closely packed layer (i.e., 1 ML is not equal to the unity of surface coverage). The procedure of preparing the mixed ice has been described previously (Watanabe et al. 2003). The H_2O and CO gases were premixed in a stainless steel bottle before deposition. Figure 1 shows the growth of H_2O and CO components on the substrate during the deposition. Although the CO component is slightly enhanced at the beginning, the ratio of H_2O/CO is approximately 4 through most of the deposition, indicating that the composition of the sample is homogeneous to a good extent. For CO-capped ice, pure H_2O ice was first produced on the substrate, and CO gas was subsequently deposited on the H_2O ice.

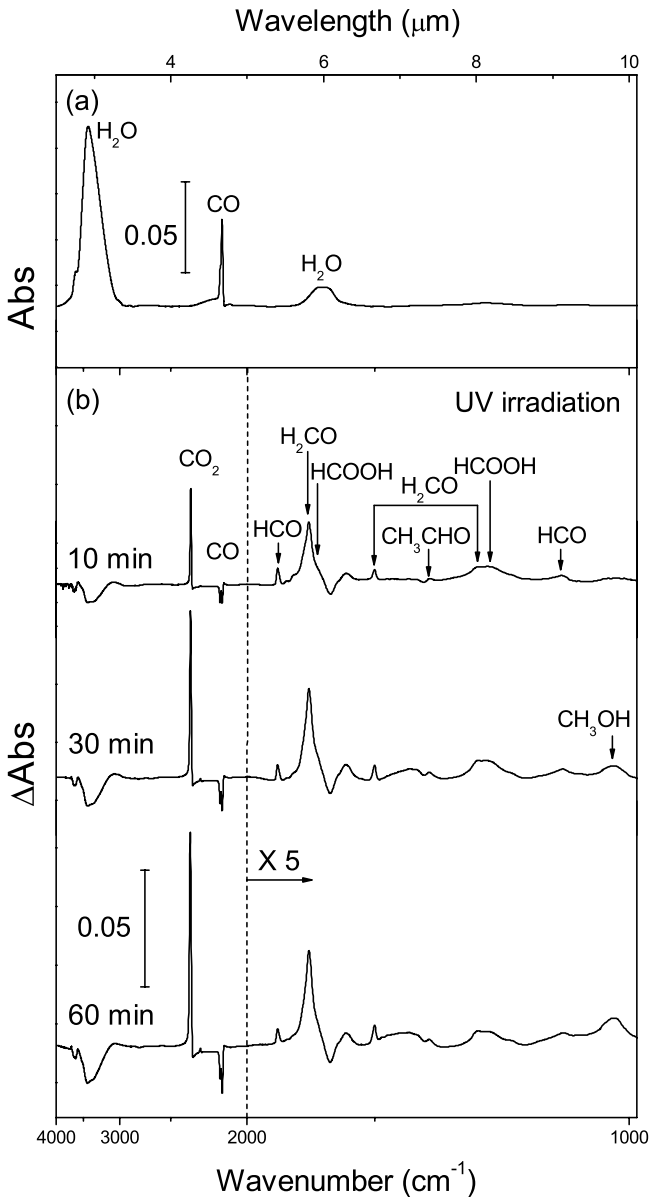


FIG. 2.—(*a*) Infrared absorption spectrum of nonirradiated mixed ice sample at 15 K. (*b*) The variation of the infrared absorption spectra of the mixed ice during UV irradiation at 15 K. The irradiation time increases from 10 (*top*) to 60 minutes (*bottom*). The lower *x*-axis is plotted in a reciprocal scale. The spectra smaller than 2000 cm^{-1} are magnified 5 times.

The UV photon source is a deuterium (D_2) lamp (L879, HAMAMATSU) with an MgF_2 window. The deuterium lamp produces the photons mainly in the energy range of the Lyman series and the Lyman band. Since the MgF_2 window excludes photons with wavelength below 115 nm, the distribution of photon wavelengths finally ranges approximately from 120 to 400 nm, with predominant peaks at around 125 and 160 nm. The photon flux is measured by a movable silicon *p-n* junction photodiode (Model AXUV-100G, IRD Inc.) placed just above the substrate. This commercial photodiode was developed for absolute photon-intensity measurements (Gullikson et al. 1996; Korde et al. 1993). It has

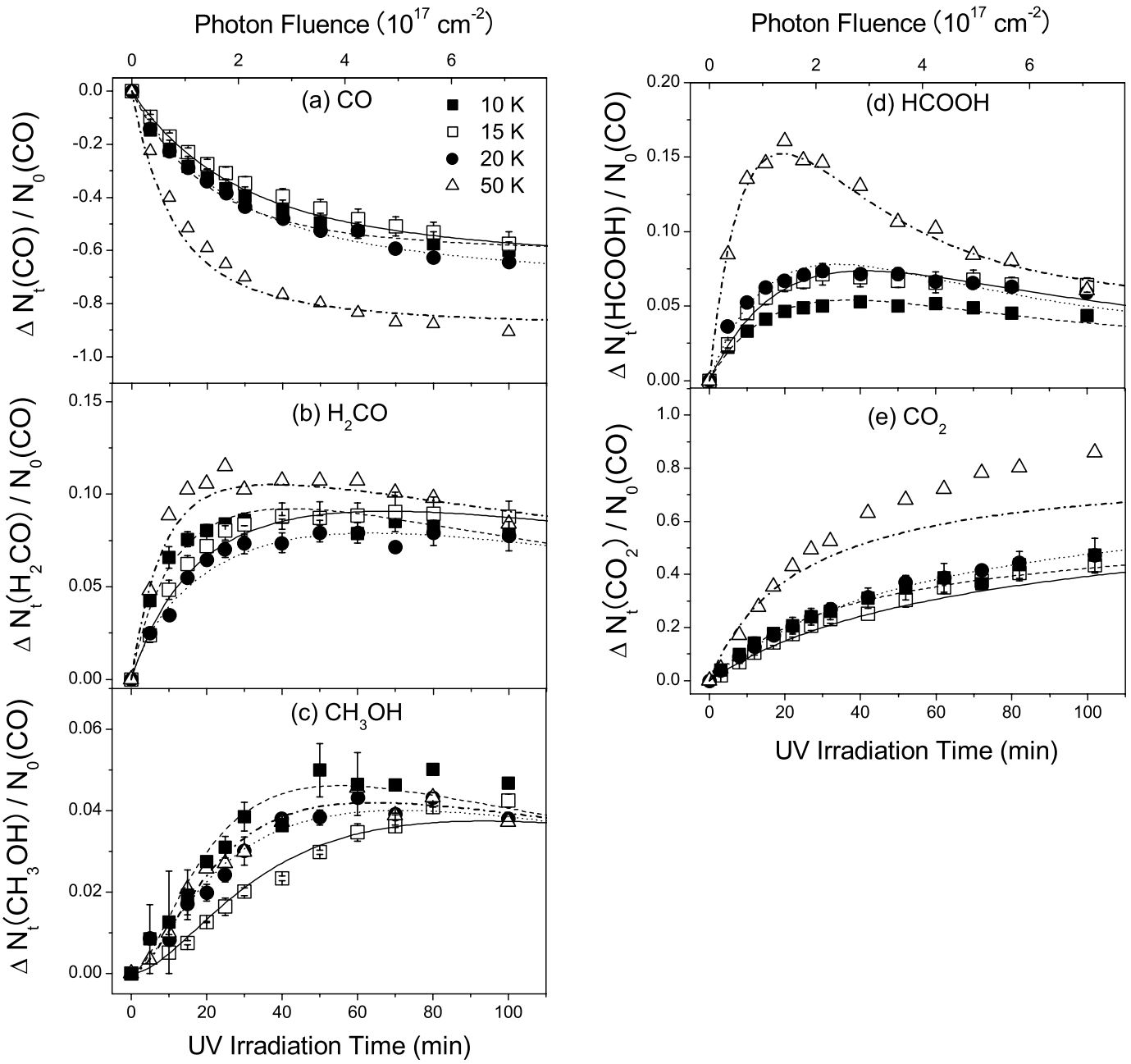


FIG. 3.—Variations in column densities, normalized to the initial CO, as a function of the irradiation time and the photon fluence for (*a*) CO, (*b*) H_2CO, (*c*) CH_3OH, (*d*) HCOOH, and (*e*) CO_2 in the mixed ice at the various surface temperatures. The error bars are statistical. Dashed, solid, dotted, and dash-dotted lines represent the results of the least-square fits for 10, 15, 20, and 50 K using eqs. (12)–(16).

been widely used in the various fields of science because of its 100% collection efficiency of photogenerated carriers (e.g., Boivin et al. 1999; Stutman et al. 1999), while the uncertainty in quantum efficiency is less than 10%. The measured photon flux of our source was 5.9×10^{13} (photons cm^{-2} s^{-1}), with photon intensity fluctuations within ~10% during the experiment. The lamp illuminates the entire area of the sample surface.

The atomic hydrogen source is of the same type as those used previously (Watanabe et al. 2006; Nagaoka et al. 2005). The hydrogen atoms were produced by the dissociation of H_2 molecules in a microwave-induced plasma inside a water-cooled Pyrex tube. The atoms from the Pyrex tube pass through a polytetrafluoroethylene tube (~8 cm) and an aluminum pipe (~40 cm in length) and finally impinge on the substrate. The aluminum pipe is connected to another cold head with a ceramic heater. In this experiment the temperature of the aluminum pipe is set to 100 K, and measured by an Au/Fe 0.07% chromel thermocouple clamped at the most downstream end of the aluminum pipe itself. The recombination of H atoms is suppressed on the aluminum surface at a low temperature (Koch & Steffens 1999) and, colliding many times with the inner walls of the pipe, they are finally thermalized at the pipe temperature (Nagaoka et al. 2007). This simple arrangement can produce low-temperature atomic hydrogen (Walraven & Silvera 1982; Perry et al. 2002). The flux of atoms was measured by a quadrupole mass spectrometer (QMS), M-400QA-M ANELVA, located just behind the substrate. To perform flux measurements, the substrate is moved down to expose the head of QMS directly to the atoms coming from the source. In our previous papers (Watanabe & Kouchi 2002b; Watanabe et al. 2003, 2004, 2006), the flux of hydrogen atoms was derived from that of

hydrogen molecules with the assumption that the dissociation efficiency of molecular hydrogen is 50%. In the present experiment, we measured a flux of H atoms of 1×10^{14} (cm^{-2} s^{-1}), as in Hidaka et al. (2007); we therefore reestimated the H fluxes of our previous works (Watanabe & Kouchi 2002b; Watanabe et al. 2003, 2004, 2006) to be approximately 4×10^{14}, 2×10^{14}, 1×10^{14}, and 1×10^{14} (cm^{-2} s^{-1}), respectively.

3. RESULTS

3.1. *Photolysis*

3.1.1. H_2O-CO *Mixed Ice*

Photolysis of the mixed ice layers was performed at 10, 15, 20, and 50 K. The ice samples were produced by deposition of premixed CO and H_2O gases at the temperatures of irradiation, except in the 50 K case. Since sublimation of CO on ice takes place approximately at 30 K, CO hardly remains in the sample deposited at 50 K; therefore, to produce the 50 K sample, the deposition was performed at 20 K, and then the temperature was raised to 50 K. When the sample is prepared in this manner, CO molecules remain at least partially trapped in H_2O ice even at 50 K. However, the H_2O/CO ratio for the 50 K sample increases to about 12, while in the other cases it is about 3 times smaller. Figure 2 shows the infrared absorption spectra of the nonirradiated and UV-irradiated samples at 15 K, for different irradiation times (total UV fluence). In the spectra of the irradiated samples, the most prominent peak is at 2346 cm^{-1}, indicating the efficient production of CO_2 by photolysis. This result is consistent with previous works on the photolysis of ice containing CO and H_2O (e.g., d'Hendecourt et al. 1986; Allamandola et al. 1988; Grim et al. 1989; Watanabe & Kouchi 2002a). We can also see the formation of formic acid (HCOOH) (1705 and 1220 cm^{-1}), H_2CO (1722, 1502, and 1249 cm^{-1}), and CH_3OH (1020 cm^{-1}). These species were not detected in our previous experiment (Watanabe & Kouchi 2002a), because of the lower S/N of the FTIR equipment in that experiment. Only at short irradiation times do we also see some small peaks assigned to HCO (1850 and 1098 cm^{-1}) and acetaldehyde (CH_3CHO) (1354 cm^{-1}), and two unidentified peaks at 1808 and 1784 cm^{-1}; such peaks are less relevant, and in spite of their potential interest for investigating the chemical complexity at the low UV doses, we will ignore them in the present paper. The same peaks were observed at all temperatures. Schutte et al. (1999) observed the formation of the same molecules in their experiment on the photolysis of H_2O-CO binary ice. A very small peak with absorbance of less than 0.002 was observed at around 2850 cm^{-1}. This peak can be attributed to H_2O_2. Using the band strength from the literature (Moore & Hudson 2000), the column density of observed H_2O_2 is estimated to be less than 1% of that of the initial CO.

In Figure 3, the column densities for CO_2, HCOOH, H_2CO, and CH_3OH at the various temperatures are plotted as a function of the irradiation time. The column densities were obtained by the area of the peaks and the absorption coefficients. The absorption coefficients adopted for the main peaks are 7.6×10^{-17} (~2350 cm^{-1}), 6.7×10^{-17} (~1710 cm^{-1}), 9.6×10^{-18} (~1722 cm^{-1}), and 1.6×10^{-17} cm $molecule^{-1}$ (~1020 cm^{-1}) for CO_2 (Gerakines et al. 1995), HCOOH (Schutte et al. 1999), H_2CO (Schutte et al. 1993), and CH_3OH (Kerkhof et al. 1999), respectively. Since the main peaks of HCOOH and H_2CO overlap at around 1720 cm^{-1}, the column density of H_2CO was determined using the second peak (1502 cm^{-1}). The absorption coefficient of the second peak is approximately 0.34 times that of the main one. The column density of HCOOH was obtained by subtracting the contribution of the main peak of H_2CO from the peak at 1710 cm^{-1}. Although CH_3CHO has a band around 1720 $cm^{-1}$with an absorption coefficient similar to that at 1354 cm^{-1}, it is negligible. One can see in Figure 3 that the amount of CO depletion is almost consistent with the sum of CO_2, HCOOH, H_2CO, and CH_3OH yields. This suggests that all of the main products are counted.

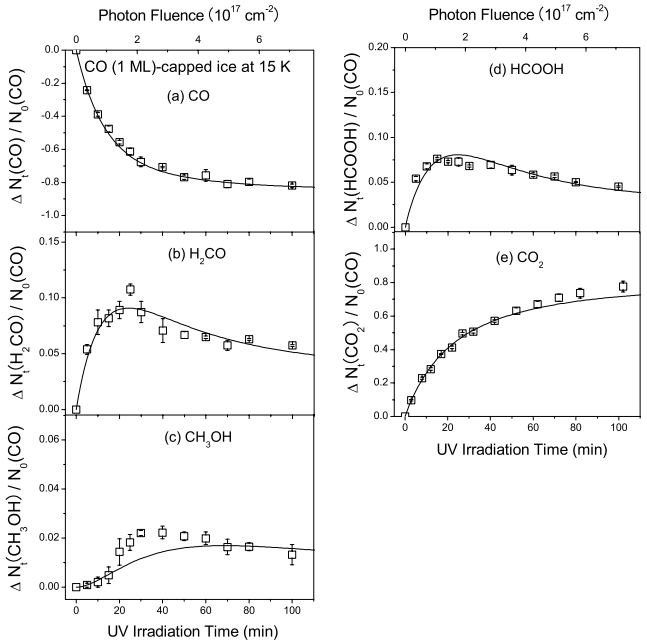


FIG. 4.—Variations in column densities normalized to the initial CO for (*a*) CO, (*b*) H_2CO, (*c*) CH_3OH, (*d*) HCOOH, and (*e*) CO_2 in the CO (1 ML)-capped ice at 15 K. Solid lines represent the results of the least-square fits using eqs. (12)–(16).

3.1.2. CO-*Capped* H_2O *Ice*

In the experiment with H_2O-CO mixed ice, reactions occur not only at the surface of ice but also in the bulk. To investigate reactions occurring only at the interface with vacuum, a CO-capped water ice was prepared and irradiated at 15 K. The observed products are the same as those detected in the case of H_2O-CO mixed ice. Variations in the column densities of CO, CO_2, H_2CO, CH_3OH, and HCOOH are plotted as a function of the irradiation time in Figure 4. The main product is CO_2 again. CH_3OH follows H_2CO formation and reaches the maximum after about 35 minutes from the beginning of the UV irradiation.

3.2. *Hydrogenation*

Although the experiments with CO hydrogenation on the various types of samples have been performed (Watanabe et al. 2004, 2006; Hidaka et al. 2004), we performed the experiments of CO hydrogenation at 15 K again for the H_2O-CO mixed ice and the CO (1 ML)-capped ice to cross-check the validity of the previous measurements. All the results obtained in this case are consistent with those of the experiments we performed previously. Infrared absorption spectra for the mixed ice irradiated with increasing fluences of H atoms and changes in column densities for CO, H_2CO, and CH_3OH are shown in Figures 5 and 6, respectively. The successive formation of H_2CO and CH_3OH was observed with the consumption of CO. In Figure 5*b*, the dip labeled A at 3660 cm^{-1} corresponds to the decrease of O—H stretching band arising from the interaction of H_2O and CO (Givan et al. 1997). The absorbance of this band decreased due to the consumption of CO neighboring H_2O. The peaks B and C cannot be assigned, but are probably OH bands of either H_2O or CH_3OH perturbed by the

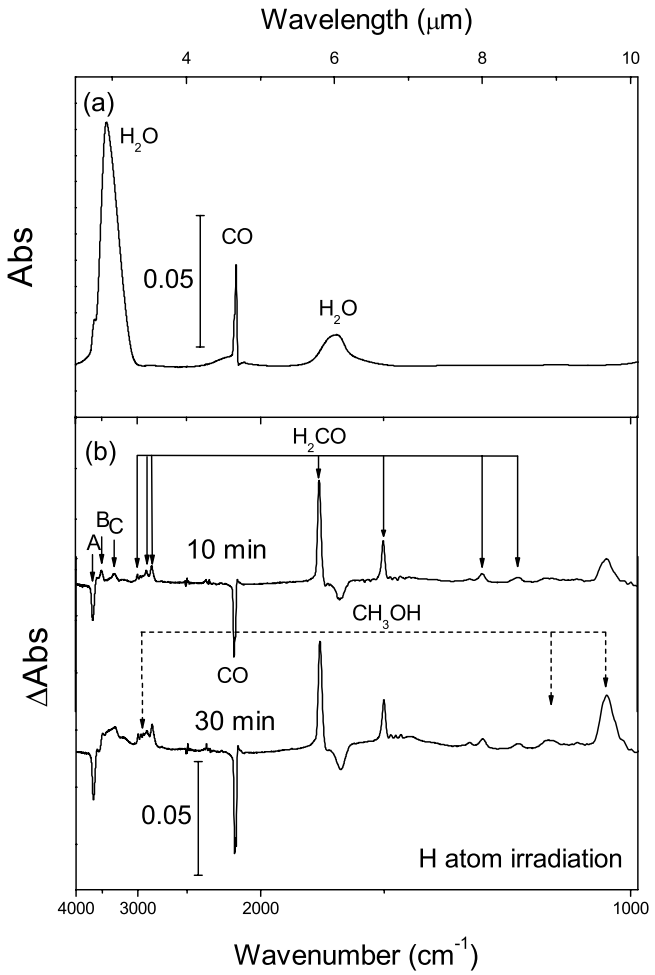


FIG. 5.—(*a*) Infrared absorption spectrum of nonirradiated mixed ice sample at 15 K. (*b*) Variation of infrared absorption spectra of the mixed ice during H atom irradiation at 15 K. The irradiation time are 10 (*top*) to 30 minutes (*bottom*). The lower *x*-axis is plotted in the reciprocal scale. The solid and dashed arrows represent H_2CO and CH_3OH, respectively. See text for the meaning of arrows A, B, and C.

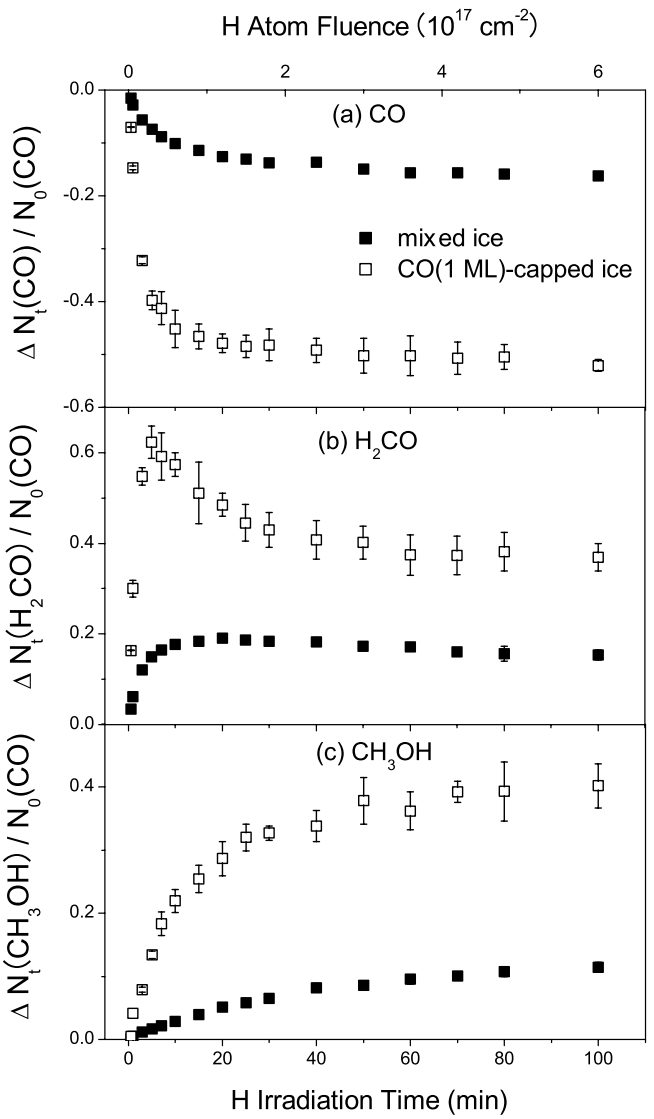


FIG. 6.—Variation in column densities normalized to the initial CO as a function of the irradiation time and the H atom fluence for (*a*) CO, (*b*) H_2CO, and (*c*) CH_3OH in the two types of samples at 15 K.

interaction of H_2O, CH_3OH, and H_2CO. The plot of CH_3OH (Fig. 6*c*) does not have a maximum, unlike the UV irradiation case, because no significant destruction process exists.

3.3. *Co-irradiation of Photons and* H *Atoms*

In molecular clouds, photons and H atoms hardly encounter simultaneously at the single molecule on the grain surface. Therefore, in principle, the chemical evolution on grains can be reproduced by the model using the set of individual data for hydrogenation and photolysis experiments. However, there could be, at least in principle, molecules that require a combination of photolysis and hydrogenation to be produced, and that cannot be produced only by a series of photo-induced reactions or by sole hydrogenation. To explore this possibility, it is necessary to perform the experiment of simultaneous irradiation of the sample with photons and H atoms. Furthermore, there are environments, such as in the early stages of star formation or in the external regions of the so called "corinos" (Bottinelli et al. 2004), when the evaporation of ice mantle has not yet started and where a co-irradiation of icy mantles by UV photons and H atoms may take place. Corinos represent an important stage of the formation of solar type stars and their planetary systems. It is very difficult to determine the rate constants and activation energies for every process in individual irradiation experiments, so detailed models for tracing the chemical evolution are not yet feasible. For this reason, we performed our experiment on the co-irradiation of various types of samples to UV and H atom at 15 K. In this experiment, H_2 from both the undissociated fraction coming from the source and the recombination of landing H atoms would partly remain on the surface. However, this H_2 coverage would not affect photolysis, because H_2 is almost transparent to photons in the energy range of our lamp. For hydrogenation, rapid recombination of H atoms might compete negatively with the hydrogenation process of CO and its daughter molecules, reducing the actual rates of these processes.

All observed products on the co-irradiation with UV photons and H atoms are the same as we found in separate photolysis and hydrogenation experiments. No co-irradiation-specific products were found. The column densities of CO and the main products, CO_2, HCOOH, H_2CO, and CH_3OH, are plotted in Figure 7.

4. DISCUSSION

4.1. *Photolysis*

For both samples of H_2O-CO mixed ice and CO-capped H_2O ice, the dominant product is CO_2. Since CO is not dissociated by

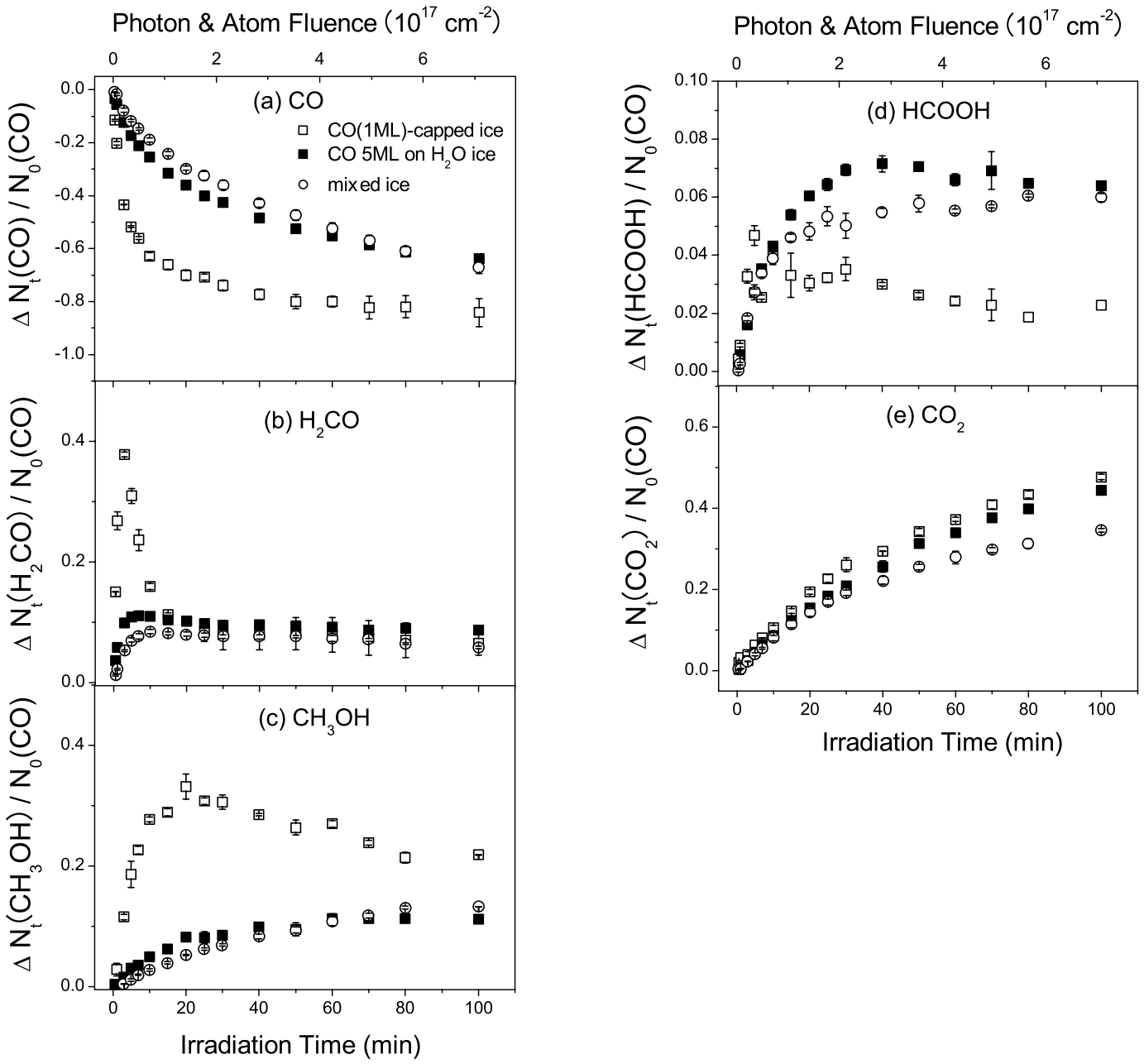


FIG. 7.—Variation in column densities for (*a*) CO, (*b*) H_2CO, (*c*) CH_3OH, (*d*) HCOOH, and (*e*) CO_2 due to the co-irradiation of the various types of samples with UV and H atom at 15 K.

the UV photons of the energies used in the present experiment, as described previously (Watanabe & Kouchi 2002a), CO_2 molecules must be formed via the reaction sequence

$$H_2O + h\nu \rightarrow OH + H \quad (1)$$

and

$$CO + OH \rightarrow CO_2 + H. \quad (2)$$

Alternatively, CO_2 could be produced by the sequence

$$H_2O + h\nu \rightarrow O + H_2 \quad (3)$$

and

$$CO + O \rightarrow CO_2. \quad (4)$$

Reaction (3) is a well known photodissociation channel in gas phase. This channel is only 1% of the total dissociation process for photon energy lower than 8.5 eV (Stief et al. 1975), but grows to be 10% at 10.2 eV (Slanger & Black 1982) in the gas phase. We consider that the direct formation of O atom, reaction (3), can proceed easily even on the surface, where dangling H atoms can bend freely, whereas it seems difficult in bulk because H_2O is surrounded by the others in all directions. Another possible route for CO_2 formation is reaction between ground and photoexcited states of CO molecules (i.e., $CO + CO^* \rightarrow CO_2 + C$). However, this process must be negligible, because the cross section is of the order of 10^{-20} cm^2 (Gerakines et al. 1996), or 10^{-19} cm^2 (Loeffler et al. 2005), which is approximately 1–2 orders of magnitude smaller than that of CO_2 formation obtained in the previous photolysis experiment (Watanabe & Kouchi. 2002a).

The yields of H_2CO, HCOOH, and CH_3OH are comparable with each other. CH_3OH appears to be behind the increase of H_2CO, supporting its formation via the following reactions of successive H addition to CO after photodissociation reaction (1):

$$CO + H \rightarrow HCO \quad (5)$$

$$HCO + H \rightarrow H_2CO \quad (6)$$

$$H_2CO + H \rightarrow CH_3O \text{ (or } CH_2OH) \quad (7)$$

$$CH_3O + H \rightarrow CH_3OH. \quad (8)$$

No peaks were observed around the wavenumbers reported for the peaks of CH_3O on the surface (Sim et al. 1995) and of CH_2OH in the Ar matrix (Jacox 1981). Although the absorption coefficients of solid CH_3O and CH_2OH are unknown, we expect that the absorption coefficients are not far from that of CH_3OH, because those species have C—O and/or O—H bonds. Therefore, we conclude that since the rate of reaction (7) is much slower than that of radical-radical reaction (8), the number densities of CH_3O and CH_2OH are under the detection limits. An alternative route to reaction (1) in producing the necessary H atoms is provided by reaction (2). The simplest pathway to the synthesis of HCOOH is given by the direct reaction of HCO with OH, which are formed by reactions (5) and (1):

$$HCO + OH \rightarrow HCOOH, \quad (9)$$

as already suggested by Hudson & Moore (1999), but of course other formation pathways are not excluded. Photolysis actually produces a quite complex network of reactions, because primary products are also photodissociated in their turn, and enter the network.

In Figure 3, we can see that CO depletions converge to some values (saturation values). The saturation value changes only a little by 20 K, but jumps at 50 K. The drastic increase of the saturation value to $\sim$0.9 at 50 K should be attributed to the high ratio of H_2O/CO rather than to the temperature. In fact, in the previous experiment (Watanabe & Kouchi 2002a), the sample had an initial abundance ratio $H_2O/CO \sim 10$, and the obtained saturation value was $\sim$0.9 even at 12 K. As a matter of fact, most CO molecules are isolated in the H_2O matrix at high H_2O/CO ratios, while a significant fraction of CO molecules aggregate at low H_2O/CO ratios. Therefore, OH, the photodissociation product of H_2O, reacts much more easily with the neighboring CO molecules isolated in H_2O than with CO that are inside CO aggregates, and hence surrounded by other CO molecules (CO-aggregate effect). Since the dominant channel of CO loss occurs through the production of CO_2 via reaction (2), the saturation values are governed by this CO-aggregate effect, and also by the balance between CO loss (reaction [2]) and reformation of CO due to photodissociation of CO_2 ($CO_2 \rightarrow CO + O$). The higher yield of HCOOH at 50 K than at 10–20 K must be due to the same reason as above: the production of HCOOH also requires reaction with OH.

For H_2O-CO mixed ice, after an irradiation of approximately 80 minutes, the abundance of CH_3OH slightly decreases (see Fig. 3*c*). This must be due to the photodissociation of CH_3OH. Such a feature is more evident in CO-capped ice. CH_3OH reaches a maximum after about 35 minutes from the beginning of the UV irradiation, as can be seen in Figure 4*c*. This maximum would appear to be due to the balance between the formation and the photodissociation rates. All species (except CO) suffer photodissociation; therefore, the plots of the products in Figures 3 and 4 do not give pure formation rates, but the net rates including destruction. Photoabsorption cross sections of H_2CO and CH_3OH are approximately 1 order of magnitude larger than those of CO_2 in the energy range of our D_2 lamp (Cheng et al. 2002; Yoshino et al. 1996; Suto et al. 1986). Since the photodissociation cross section is similar to the photoabsorption cross sections at these photon energies, the yields of H_2CO and CH_3OH tend to be more suppressed than the CO_2 yield, due to the competition between the formation and photodestruction.

When comparing the results for the capped ice with those for the mixed ice, the main difference consists in the low yields of H_2CO, CH_3OH, and HCOOH relative to CO_2 for the capped ice. The behavior and yield of CO_2 is quite comparable to those for mixed ice, while H_2CO and CH_3OH are produced immediately at the beginning of the irradiation and saturate at a lower value than in the case of mixed ice. The formation of H_2CO, HCOOH, and CH_3OH requires reactions of CO with H atoms (reactions [3]–[6]). It is reasonable to accept that the lower yields of H_2CO, CH_3OH, and HCOOH in the CO-capped ice than in the mixed ice result in reactions of H atoms. H atoms produced in H_2O photodissociation by UV irradiation have significant kinetic energy; in fact, for the dissociation into the main channel H + OH ($X^2\Pi$, $A^2\Sigma^+$) in gas phase (Dutuit et al. 1985) and due to the mass ratio H/OH, H atoms produced by reaction (1) typically have a high kinetic energy excess between 1 and 5 eV. Reaction (2) yields H atoms of about 1 eV. Those energetic H atoms would cause the following effects: first, the energetic H atoms produced at the surface could easily escape into vacuum without reactions; second, the energetic H atoms could destroy already synthesized HCO and H_2CO molecules through the abstraction reactions

$$HCO + H \rightarrow CO + H_2 \quad (10)$$

and

$$H_2CO + H \rightarrow HCO + H_2. \quad (11)$$

To discuss the difference in reactions of H atoms between the mixed ice and the CO-capped ice, we hereafter exclude HCOOH, because the formation of this molecule requires reactions involving both H and OH. It is easy to understand that the first effect causes the lower relative yields of H_2CO and CH_3OH to CO_2 for the CO-capped ice than for the mixed ice. Since CO molecules in the CO-capped ice are located only at the surface, the efficiencies of H_2CO and CH_3OH formation become lower in the CO-capped ice case than in the mixed ice case. On the other hand, the efficiency of CO_2 formation would not depend on the type of ice. Since the initial kinetic energy of the OH fragment in each H_2O photodissociation process is only 1/17 that of the H atom, OH would stay much closer to the dissociation site than H atoms without escaping, and therefore still react with neighboring CO. For this reason, CO_2 formation (reaction [2]) proceeds efficiently for both the CO-capped ice and the mixed ice. As a result, the relative yields of H_2CO/CO_2 and CH_3OH/CO_2 become smaller for the CO-capped ice. Furthermore, for the second effect, abstraction reactions (10) and (11) to destroy H_2CO and CH_3OH would be more enhanced in the CO-capped ice than in the mixed ice case. Such an enhancement occurs because the average kinetic energy of H atoms (produced by the photodissociation of water) is higher at a reaction site on the surface than at one in the bulk, where binary collisions with surrounding H_2O and CO molecules slow down and quickly thermalize the energetic H fragments. Reactions (10) and (11) would compete with formation reactions (6) and (7), reducing the yields of H_2CO, HCOOH, and particularly that of CH_3OH. The activation energies of reactions (10) and (11)

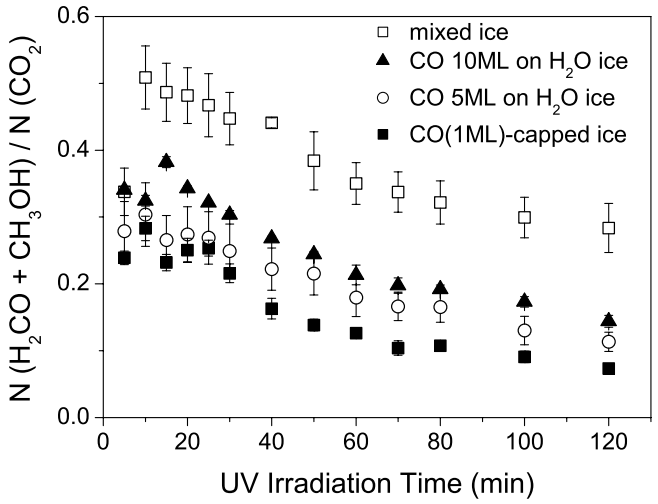


FIG. 8.—Ratio of photo CO_2 yields to the sum of H_2CO and CH_3OH for the various types of samples at 15 K.

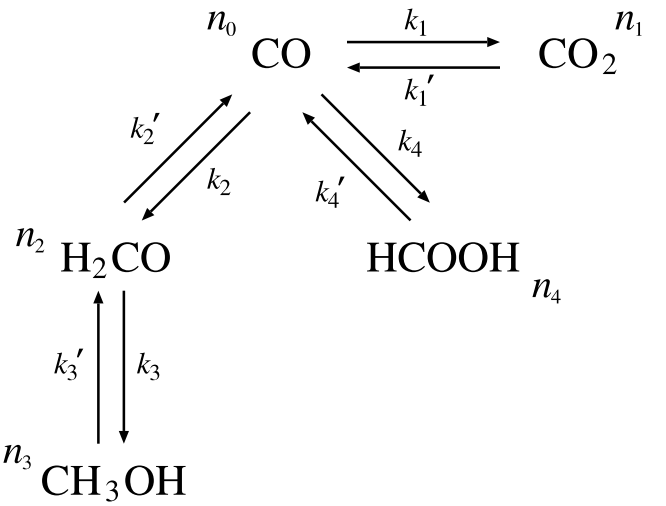


FIG. 9.—Effective reaction network for photolysis; n_i is column density, and k_n and k_n' represent the effective reaction rates for forward and reverse processes, respectively. Reaction partners of H and OH radicals are not shown and are assumed to be sufficiently supplied by the photodissociation of H_2O in the reaction systems.

are substantially higher than those of reactions (6) and (7) (Woon 2002), and therefore hardly proceed with *thermal* H atoms (Hidaka et al. 2004). For the CO-capped ice, CO and the other reactants such as H_2CO are located at the surface of H_2O and consequently react with the energetic H atoms mainly produced near the surface. For the mixed ice, since the H atoms responsible for the reactions with CO are produced predominantly in the ice bulk and lose the kinetic energy before the reactions, the dominant pathway of H atoms would be the formation of HCO and H_2CO, leading to CH_3OH, rather than the destruction of those.

According to the scenario presented above, when *thermal* H atoms directly impinge on CO, both in the mixed ice and in the CO-capped ice, H_2CO and CH_3OH are produced efficiently. In fact, as described in § 3.2, significant yields of H_2CO and CH_3OH are obtained in the experiment of H atom irradiation of the CO-capped ice. To further confirm the above effects, we irradiated CO/H_2O double-layer samples prepared by depositing approximately 5 or 10 ML of solid CO on predeposited 30 ML of pure H_2O ice. In these samples, the energetic H atoms emitted toward the solid CO are expected to lose their kinetic energy inside the solid CO and finally produce H_2CO via reactions (5) and (6). It was found that the relative yields of H_2CO/CO_2 and CH_3OH/CO_2 both increase with the thickness of CO on H_2O ice. In Figure 8, we plot the ratio of sum of column densities of H_2CO and CH_3OH to column density of CO_2 for the all type of samples. It is clearly seen that the sum of H_2CO and CH_3OH yields relative to CO_2 for the double-layer samples become larger than those for CO-capped ice.

It is not easy to obtain the information on elementary processes such as branching ratios among reaction channels and rate constants from this kind of simulation experiment. The standard approach to determining the exact reaction channels is to construct a kinetic model for the system and to fit the data. However, unlike the gas phase, determination of absolute reaction channels and rate constants is extremely difficult for the solid phase reactions, for several reasons: (1) single-collision conditions are not expected in solid phase; (2) measurements of column densities for some radicals, infrared inactive molecules, and atoms are difficult; (3) reactions in solid phase are too complicated to construct the exact reaction network; and (4) a major difficulty is that reactions strongly depend on the structure and the composition of the surface and bulk (Watanabe et al. 2006; Hidaka et al. 2007), in other words, molecules cannot move freely in solid phase. Therefore, we propose the simple reaction network shown in Figure 9 and estimate the relative effective reaction rates. In this model, the intermediate (and those formation processes) and minor products are neglected, and only effective forward and reverse processes are considered. The forward processes represent H (reactions [5]–[8]) or OH (reactions [2] and [9]) addition, while the reverse processes include photodissociation and abstraction reaction by H (reactions [10] and [11]). We adopt effective rate constants k_n and k_n', representing all the forward and reverse processes, respectively. On the assumption that reactants H and OH are continuously fed sufficiently by photodissociation of H_2O, the reaction network provides the following rate equations:

$$\frac{dn_0}{dt} = -(k_1 + k_2 + k_4)n_0 + k_1'n_1 + k_2'n_2 + k_4'n_4 \quad (12)$$

$$\frac{dn_1}{dt} = k_1n_0 - k_1'n_1 \quad (13)$$

$$\frac{dn_2}{dt} = k_2n_0 - (k_2' + k_3)n_2 + k_3'n_3 \quad (14)$$

$$\frac{dn_3}{dt} = k_3n_2 - k_3'n_3 \quad (15)$$

$$\frac{dn_4}{dt} = k_4n_0 - k_4'n_4, \quad (16)$$

where n_0, n_1, n_2, n_3, and n_4 are the relative column densities of CO, CO_2, H_2CO, CH_3OH, and HCOOH, respectively.

After solving the equations, we fitted the data for mixed and CO-capped ices. In fitting the CO data, the CO-aggregate effect described above was considered. That is, the saturation value of CO depletion for the present mixed ice is governed by not only the balance between forward (CO_2 formation) and reverse (photodissociation of CO_2) processes, but also the CO-aggregate effect. We assumed that the saturation value of 0.9 for the mixed ice at the high CO/H_2O ratio of 0.1 (data for 50 K and Watanabe & Kouchi 2002a) is purely determined by the balance between forward and reverse processes. The results of fittings are shown in Figures 3 and 4, and the effective rates obtained are listed in Table 1. Below 20 K, each relative rate for mixed ice depends little on the temperature. Since photolysis is an energetic process, reaction rates tend to be temperature-independent as long as the structure and composition of the ice are similar. This feature is one of the major

TABLE 1
Effective Reaction Rates for the Photolysis Processes Shown in Figure 9

Temperature	k_1	k_2	k_3	k_4	k_1/k_1'	k_2/k_2'	k_3/k_3'	k_4/k_4'
Mix 10 K	1	0.7 ± 0.1	2.7 ± 0.5	0.3 ± 0.1	5.7 ± 2.0	0.45 ± 0.08	0.5 ± 0.1	0.22 ± 0.05
15 K	1	0.6 ± 0.1	1.9 ± 0.4	0.6 ± 0.1	6.8 ± 4.1	0.4 ± 0.1	0.4 ± 0.1	0.23 ± 0.04
20 K	1	0.5 ± 0.1	4.8 ± 0.9	0.5 ± 0.1	5.5 ± 2.5	0.31 ± 0.06	0.5 ± 0.1	0.20 ± 0.04
50 K	1	0.4 ± 0.1	0.8 ± 0.2	0.7 ± 0.1	6.2 ± 1.7	0.5 ± 0.1	0.4 ± 0.1	0.4 ± 0.1
Cap 15 K	1	0.3 ± 0.1	0.2 ± 0.1	0.3 ± 0.1	6.5 ± 1.7	0.3 ± 0.1	0.3 ± 0.1	0.2 ± 0.1

Notes.—Rates are normalized to k_1 at each temperature. The absolute values of k_1 are $2.0 \pm 0.1 \times 10^{-2}$, $1.3 \pm 0.1 \times 10^{-2}$, $1.5 \pm 0.1 \times 10^{-2}$, $3.4 \pm 0.3 \times 10^{-2}$ minute^{-1} for the mixed ice at 10, 15, 20, and 50 K, and $3.6 \pm 0.3 \times 10^{-2}$ minute^{-1} for the capped ice at 15 K, respectively. The ratios of forward rates to reverse rates, k_n/k_n', are also listed.

difference from hydrogenation, in which reaction rates strongly depend on the temperature even within 10–20 K. For the mixed ice at 50 K, reaction rates for CO_2 and HCOOH formation, k_1 and k_4, are enhanced relative to k_2 and k_3. This would be due to the effect of the lower CO/H_2O ratio in 50 K sample, as discussed above. The reaction with photodissociated OH would be more sensitive to the CO/H_2O ratio in the sample than the reaction with H atoms. For the CO-capped ice at 15 K, reaction rates of H_2CO, CH_3OH, and HCOOH formation (k_2, k_3, and k_4) are smaller than those for the mixed ice, supporting the above scenario for the effect of energetic H atom (H escape from the surface). It is evident that the effective rates strongly depend on the structure and composition of the sample ice. The difference between the data and fits for CH_3OH in the CO-capped ice (Fig. 4*c*) and CO_2 in the mixed ice at 50 K (Fig. 3*e*) are relatively large. The reason for that is not clear. Since reactions depend on the structure of the sample, the scheme of reactions for the CO-capped ice may differ from those for the mixed ice. We may need additional routes in our reaction network. Furthermore, it should be noted that the absorption coefficients of CO_2 in H_2O ice at 50 K have not been measured, and would be somewhat different from those in literature.

4.2. *Hydrogenation*

The attenuation of CO column density is smaller than the sum of the increase in H_2CO and CH_3OH. This could be due to errors in the estimated absorption coefficients. More precisely, the absorption coefficient estimated for CO could be relatively larger than those for H_2CO and CH_3OH. In Figure 7, we can see that the CO depletion rate and the saturation value for CO-capped ice are larger than those for the mixed ice. The higher saturation value can be explained by the number of CO molecules located within the reach of H atoms. For CO-capped ice, most of the CO is exposed at the surface of H_2O ice and accessible by impinging H atoms, while in the case of the mixed ice a significant amount of CO is embedded in ice and cannot be reached easily by H atoms. The CO depletion rate depends on the CO coverage of H_2O ice (Hidaka et al. 2007). As described in § 2, the coverage is not unity even for CO-capped ice, and the composition at the surface is still H_2O rich. In our experimental conditions, the CO coverage of CO-capped ice was found to be smaller than that of mixed ice (Hidaka et al. 2007), leading to a higher rate of CO depletion. The existence of H_2O at the surface enhances the CO depletion, probably due to the higher sticking coefficient of H atom on H_2O ice than on solid CO (Watanabe et al. 2006). Once a higher number density of H atom is obtained at the surface, reaction (5) proceeds more efficiently.

4.3. *Photolysis vs. Hydrogenation*

The major difference between photolysis and hydrogenation is in the number of products. Photolysis yields CO_2, HCOOH, H_2CO, CH_3OH, CH_3CHO, and probably undetectably small amount of other products, while only H_2CO and CH_3OH are obtained by hydrogenation. The amount of CO that reacts after sufficient irradiation, namely the saturation value of CO, is larger in the case of photolysis than in the case of hydrogenation, because photolysis occurs not only at the surface but also in the bulk of the ice, while hydrogenation proceeds only at ice surface within the reach of H atoms. However, since the main channel of photolysis is the production of CO_2, the efficiency of H_2CO and CH_3OH formation (yields per photon and per atom) and the total amount of formaldehyde and methanol produced by hydrogenation are higher than for photolysis in any type of ice sample (see Figs. 3, 4, and 6). In particular, the difference in the efficiency and the total yields between hydrogenation and photolysis becomes largest for the CO (1 ML)-capped ice, where most CO molecules are exposed at the surface.

4.4. *Co-irradiation of Photons and* H *Atoms*

One can easily find several interesting features in co-irradiation, when a comparison is performed with the results of individual irradiation using H and UV at 15 K. Let us first analyze the behavior of CO (see Figs. 3*a*, 4*a*, 6*a*, and 7*a*); the attenuation rate in the co-irradiation case is close to the sum of the attenuation rates for the individual H and UV irradiations. The saturation value of CO attenuation is almost the same as that for UV irradiation, indicating that the total amount of CO that reacts is determined mainly by photolysis rather than by hydrogenation. This is understandable, because photolysis takes place not only at the surface but also inside ice, while hydrogenation is limited to within the reach of H atoms, i.e., only near the surface. For CO_2, the production rate and the yield due to co-irradiation are essentially similar to those obtained by UV irradiation; that is, hydrogen atoms do not perturb CO_2 production. The yields of the other products cannot be reproduced by simply summing those for the single UV and H atom irradiations. As far as HCOOH is concerned, the yields due to co-irradiation remain slightly lower than those due to UV irradiation alone. This feature seems to support the formation route of HCOOH through reactions (5) and (9). In the co-irradiation experiment, the number of H atoms available is much larger than that produced only by UV photodissociation, because of the additional H irradiation. Therefore, after HCO formation, H addition reactions (6) and (7) to produce H_2CO must be relatively enhanced with respect to HCOOH formation via reaction (9), compared to the single UV irradiation. For H_2CO and CH_3OH, the results of co-irradiation demonstrate that photons effectively work for destruction rather than formation when UV irradiation is combined with H atom irradiation. In fact, the yields of H_2CO and CH_3OH for co-irradiation are smaller than those for the single irradiation of H atoms in all types of samples. This feature is remarkable especially for CO (1 ML)-capped ice. As shown in Figure 7*c*, the CH_3OH plot for co-irradiation of CO (1 ML)-capped ice has a maximum due to

TABLE 2
Molecular Abundances Relative to CO Obtained by Ice Mantle Observations and the Present Experiment at 15 K

Molecule	W33A	Elias29	Elias16	UV		H		Co-irradiation	
				Mix	Cap	Mix	Cap	Mix	Cap
CO	100	100	100	100 (100)	100	100	100	100	100
CO_2	163	394	97	108 (960)	457	...	...	123	298
H_2CO	38	36	...	22 (93)	34	18	77	24	41
CH_3OH	207	312	12	11 (41)	7.7	14	84	61	137
HCOOH	46	1.8	...	16 (67)	27	...	...	18	14

Notes.—Observational data for molecular clouds toward the high-mass protostar (W33A), low-mass protostar (Elias 29), and the field star (Elias 16) are from Gibb et al. (2004). Experimental data after an irradiation time of 100 minutes were adopted. The values in parenthesis represent the data for UV irradiation of mixed ice at 50 K.

photodissociation at around 20 minutes irradiation time, which is earlier than for the single UV irradiation (see Figs. 3*c* and 4*c*). In the co-irradiation of CO (1 ML)-capped ice, the formation of CH_3OH proceeds predominantly by hydrogenation and terminates at an early irradiation stage, after which photodissociation due to UV irradiation is more relevant.

5. ASTROPHYSICAL IMPLICATIONS

Since the visual extinction is typically larger than 10 mag in molecular clouds where the solid-phase molecules were observed, the interstellar UV radiation is greatly attenuated at the interior. At such depths, cosmic-ray-induced photons from hydrogen molecules become predominant. The total UV flux, the sum of the cosmic-ray-induced and attenuated interstellar photons, was calculated by Cecchi-Pestellini et al. (1995) as a function of geometrical depth of a cloud; they found that the flux increases outward from approximately 10^4 cm^{-2} s^{-1} at the center of core. The emission spectrum of cosmic-ray-induced photons should be similar to that of our D_2 lamp, i.e., Lyman series and Lyman band are expected (Gredel et al. 1987). Although photons at approximately 90–110 nm were excluded by the window material in our experiment, these photons would exist and dissociate CO molecules in actual clouds. This effect of CO photodissociation cannot be evaluated in the present experiment. Assuming a UV photon flux of 4×10^4 cm^{-2} s^{-1}, a number density of 1 cm^{-3}, and a temperature of 10 K for H atom in molecular clouds, we find that the fluences of photons and H atoms for 1×10^5 and 5×10^5 yr are 1.3×10^{17} and 6.5×10^{17} cm^{-2}, respectively. Those fluences are achieved approximately after an irradiation of 20 and 100 minutes in the present experiments. The abundances of CO, CO_2, HCOOH, H_2CO, and CH_3OH, observed in molecular clouds, and the experimental yields at 15 K after 100 minutes of irradiation, are listed in Table 2. For convenience of comparison to observations, the experimental data shown in the table are normalized to the *remaining* (i.e., unreacted) CO, namely $\Delta N_{t=100}(\mathrm{X})/\{N_0(\mathrm{CO}) - |\Delta N_{t=100}(\mathrm{CO})|\}$. It should be noted that these values are different from the *absolute* yields, $\Delta N_{t=100}(\mathrm{X})$, and from the values normalized to the *initial* CO abundance, $\Delta N_{t=100}(\mathrm{X})/N_0(\mathrm{CO})$, used in Figures 3, 4, 6, and 7. Although the experimental values do not completely coincide with the observations, the results obtained in the case of the co-irradiation better reproduce the observations. It is obvious that the formation of CO_2 requires photolysis. Our assumed photon flux of 4×10^4 cm^{-2} s^{-1} is probably high for quiescent environments like Elias 16. The other process, CO + O (Roser et al. 2001), would contribute also to the formation of CO_2. For the formation of CH_3OH, hydrogenation is essential; it is, in fact, difficult to produce enough CH_3OH without hydrogenation. On the other hand, relatively high H_2CO abundance values can be achieved almost at the level of observations by photolysis alone.

When we compare the effectiveness of photolysis and hydrogenation in the formation of H_2CO and CH_3OH, the efficiencies of formation (number of products per single photon or per single H atom) are the fundamental parameters. In this sense, as discussed in § 4.3, hydrogenation is more efficient than photolysis. In fact, the yields of H_2CO and CH_3OH in hydrogenation are larger than those in photolysis (see Figs. 3, 4, and 6). However, relative abundances of H_2CO and CH_3OH in Table 2 strongly depend on the structure, temperature, and composition of ice, at least as much as on the difference in the types of irradiation. For example, in the case of the photolysis of mixed ice below 20 K, the maximum abundances of H_2CO and CH_3OH relative to the *remaining* CO are approximately 0.2 and 0.1, respectively. Such values are comparable to those obtained by hydrogenation. Furthermore, the relative H_2CO and CH_3OH abundances for the photolysis of mixed ice becomes about 1 and 0.4 at 50 K, where hydrogenation never proceeds because of a very low sticking coefficient of H atoms. This discrepancy between the formation efficiency and the relative abundance arises from the amount of CO consumption. Even though the yields and the formation efficiencies of H_2CO and CH_3OH are smaller, photolysis has an additional channel for CO consumption, namely CO_2 formation. When photolysis consumes CO much more than hydrogenation, the abundances of H_2CO and CH_3OH relative to the *remaining* CO can be larger than those obtained by hydrogenation despite the smaller absolute photo-yields of H_2CO and CH_3OH. Unlike hydrogenation, in the mixed ice photolysis occurs not only on the surface but also in the bulk; the remaining CO (consumption) due to photolysis is smaller (larger) than for hydrogenation. Therefore, in the mixed ice case photolysis is better than hydrogenation from the point of view of getting higher relative abundances of H_2CO and CH_3OH. The temperature and composition of ice are also important factors in determining the relative abundances. Photolysis proceeds even at high temperatures, in which CO can still be trapped in H_2O ice, while hydrogenation cannot be expected to be efficient at temperatures much higher than 20 K. Photon-induced reaction chains need as a first step photodissociation of H_2O near CO; therefore, efficiency is higher when the amount of H_2O surrounding CO is higher. In other words, the fraction of CO remnants in ice decreases with the increase of H_2O/CO ratio, leading to higher relative abundances of H_2CO and CH_3OH. In the photolysis measurements, the H_2O/CO ratio in the 50 K mixed ice is 12. The relative abundance of H_2CO is the highest in this sample, and reaches 9.3 beyond those for hydrogenation in any sample, and the observed H_2CO abundances (see Table 2).

The relative roles of photolysis and hydrogenation in the ice mantle can be summarized as follows. For H_2CO and CH_3OH, hydrogenation has a higher formation efficiency and provides higher yields than photolysis. Our experiments also show that photolysis contributes significantly the formation of those molecules,

especially H_2CO, in molecular clouds where the UV flux is above $\sim 10^4$ cm^{-2} s^{-1}. Photolysis efficiently converts CO to CO_2 and HCOOH. The relative abundances of those molecules in experiments in which only UV irradiation is performed reproduce the observations well. The relative abundances produced by photolysis strongly depend on the ratio of H_2O/CO and the structure of the ice (the location of CO in/on ice), while the abundances produced by hydrogenation are sensitive to the temperature and structure of the ice.

Extrapolating experimental results more precisely to interstellar environments is not easy, and some sophisticated modeling should be used. Such models should take into consideration that in molecular clouds, the ice mantle does not exist before irradiation, but is gradually formed while irradiation goes on. However, the present results first indicate that the irradiation of simple binary H_2O-CO ice with UV and H atoms can reproduce rather closely the observed abundances of CO, CO_2, HCOOH, H_2CO, and CH_3OH.

6. CONCLUSIONS

We performed several experiments of UV and H atom irradiation and co-irradiation of ice mantle analogs. The main results obtained in the present work are the following:

1. Hydrogenation is more efficient than photolysis in producing H_2CO and CH_3OH under conditions that are typical in molecular clouds.

2. Photolysis cannot be neglected in the formation of H_2CO and CH_3OH in molecular clouds when the UV flux is approximately $>10^4$ cm^{-2} s^{-1}.

3. Hydrogenation occurs preferentially for CO at the surface of the ice mantle, rather than over CO embedded in H_2O.

4. Photolysis produces CO_2 and HCOOH in UV fluxes larger than $\sim 10^4$ cm^{-2} s^{-1}.

5. Photolysis works more effectively for CO embedded in H_2O matrix than for apolar CO.

6. The composition and the structure of ice (polar or apolar) are as crucial in the chemical evolution of ice mantles as the grain temperature and the flux of irradiation in molecular clouds. Our results first highlight the importance of the above factors in the chemical evolution of interstellar mantles on grains. Those factors should be significantly considered in models.

7. The co-irradiation of H_2O-CO binary ice analogs with UV and H atoms reproduces observation fairly well.

This work was supported in part by a Grant-in-Aid for Scientific Research from the Japan Society for the Promotion of Science and by the Hokkaido University Grant Program for Leading Edge Research.

REFERENCES

Allamandola, L. J., Sandford, S. A., & Valero, G. J. 1988, Icarus, 76, 225
Boivin, R. L. Goetz, J. A., Marmar, E. S., Rice, J. E., & Terry, J. L. 1999, Rev. Sci. Instrum., 70, 260
Bottinelli, S., et al. 2004, ApJ, 617, L69
Cecchi-Pestellini, C., Aiello, S., & Barsella, B. 1995, MNRAS, 274, 134
Charnley, S. B., Tielens, A. G. G. M., & Rodgers, S. D. 1997, ApJ, 482, L203
Cheng, B., Bahou, M., Chen, W., Yui, C., & Lee, Y. 2002, J. Chem. Phys., 117, 1633
d'Hendecourt, L. B., Allamandola, L. J., Grim, R. J. A., & Greenberg, J. M. 1986, A&A, 158, 119
Dutuit, O., Tabche-Fouhaile, A., Nenner, I., Frohlich, H., & Guyon, P. M. 1985, J. Chem. Phys., 83, 584
Gerakines, P. A., Schutte, W. A., & Ehrenfreund, P. 1996, A&A, 312, 289
Gerakines, P. A., Schutte, W. A., Greenberg, J. M., & van Dishoeck, E. F. 1995, A&A, 296, 810
Gibb, E. L., Whittet, D. C. B., Boogert, A. C. A., & Tielens, A. G. G. M. 2004, ApJS, 151, 35
Givan, A., Loewenschuss, A., & Nielsen, C. J. 1997, J. Phys. Chem. B, 101, 8696
Gredel, R., Lepp, S., & Dalgarno, A. 1987, ApJ, 323, L137
Grim, R. J., Greenberg, J. M., de Groot, M. S., Baas, F., Schutte, W. A., & Schmitt, B. 1989, A&AS, 78, 161
Gullikson, E. M., Korde, R., Canfield, L. R., & Vest, R. E. 1996, J. Electron Spectrosc. Related Phenom., 80, 313
Hidaka, H., Kouchi, A., & Watanabe, N. 2007, J. Chem. Phys., 126, 204707
Hidaka, H., Watanabe, N., Shiraki, T., Nagaoka, A., &Kouchi, A. 2004, ApJ, 614, 1124
Hiraoka, K., Ohashi, N., Kihara, Y., Yamamoto, K., Sato, T., & Yamashita, A. 1994, Chem. Phys. Lett., 229, 408
Hudson, R. L., & Moore, M. H. 1999, Icarus, 140, 451
Jacox, M. E. 1981, Chem. Phys., 59, 213
Kerkhof, O., Schutte, W. A., & Ehrenfreund, P. 1999, A&A, 346, 990
Koch, N., & Steffens, E. 1999, Rev. Sci. Instr., 70, 1631
Korde, R., Cable, J. S., & Canfield, L. R. 1993, IEEE Trans. Nucl. Sci., 40, 1655
Loeffler, M. J., Baratta, G. A., Palumbo, M. E., Strazzulla, G., & Baragiola, R. A. 2005, A&A, 435, 587
Moore, M. H., & Hudson, R. L. 2000, Icarus, 145, 282
Nagaoka, A., Watanabe, N., & Kouchi, A. 2005, ApJ, 624, L29
Nagaoka, A., Watanabe, N., & Kouchi, A. 2007, J. Phys. Chem. A, 111, 3016
Perry. J. S. A., Gingell, J. M., Newson, K. A., To, J., Watanabe, N., & Price, S. D. 2002, Meas. Sci. Tech., 13, 1414
Pirronello, V., Biham, O., Liu, C., Shen, L., & Vidali, G. 1997a, ApJ, 483, L131
Pirronello, V., Brown, W. L., Lanzerotti, L. J., Marcantonio, K. J., & Simmons, E. H. 1982, ApJ, 262, 636
Pirronello, V., Liu, C., Roser, J. E., & Vidali, G. 1999, A&A, 344, 681
Pirronello, V., Liu, C., Shen, L., & Vidali, G. 1997b, ApJ, 475, L69
Roser, J,. Vidali, G., Manicò, G., & Pirronello, V. 2001, ApJ, 555, L61
Schutte, W. A. 1988, Ph.D. thesis, Univ. Leiden
———. 1996, in IAU Symp. 178, Molecules in Astrophysics, ed. E. F. van Dishoeck (Dordrecht: Kluwer), 331
Schutte, W. A., Allamandola, L. J., & Sandford, S. A. 1993, Icarus, 104, 118
Schutte, W. A., Gerakines, P. A., Geballe, T. R., van Dishoeck, E. F., & Greenberg, J. M. 1996, A&A, 309, 633
Schutte, W. A., et al. 1999, A&A, 343, 966
Sim, W. S., Gardner, P., & King, D. A. 1995, J. Phys. Chem., 99, 16002
Slanger, T. G., & Black, G. 1982, J. Chem. Phys., 77, 2432
Stief, L. J., Payne, W. A., & Klemm, R. B. 1975, J. Chem. Phys., 62, 4000
Stutman, D., Finkenthal, M., Soukhanovskii, V., May, M. J., Moos, H. W., & Kaita, R. 1999, Rev. Sci. Instrum., 70, 572
Suto, M., Wang, X., & Lee, L. C. 1986, J. Chem. Phys., 85, 4228
Tielens, A. G. G. M., & Whittet, D. C. B. 1997, in IAU Symp. 178, Molecules in Astrophysics, ed. E. F. van Dishoeck (Dordrecht: Kluwer), 45
Vidali, G., Roser, J. E., Manicò, G., & Pirronello, V. 2004, Adv. Space Res., 33, 6
Walraven, J. T. M., & Silvera, I. F. 1982, Rev. Sci. Instrum., 53, 1167
Watanabe, N. 2006, in Astrochemistry, ed. D. C. Lis, G. A. Blake, & E. Herbst (Cambridge: Cambridge Univ. Press), 415
Watanabe, N., & Kouchi, A. 2002a, ApJ, 567, 651
———. 2002b, ApJ, 571, L173
Watanabe, N., Nagaoka, A., Hidaka, H., Shiraki, T., Chigai, T., & Kouchi, A. 2006, Planet. Space Sci., 54, 1107
Watanabe, N., Nagaoka, A., Shiraki, T., & Kouchi, A. 2004, ApJ, 616, 638
Watanabe, N., Shiraki, T., & Kouchi, A. 2003, ApJ, 588, L121
Woon, D. E. 2002, ApJ, 569, 541
Yoshino, K., Esmond, J. R., Sun, Y., Parkinson, W. H., Ito, K., & Matsui, T. 1996, J. Quant. Spectrosc. Radiat. Transfer, 50, 53